

The Bethe–Salpeter equation: a first-principles approach for calculating surface optical spectra

M Palumbo¹, O Pulci¹, R Del Sole¹, A Marini², P Hahn³, W G Schmidt³
and F Bechstedt³

¹ INFN, Dipartimento di Fisica Università di Roma ‘Tor Vergata’, Via della Ricerca Scientifica 1, I-00133 Roma, Italy

² Departamento da Física da Materialas, Facultad de Ciencias Quimicas UPV/EHU, Centro Mixto CISC-UPV/UHV and Donostia International Physics Center, E-20018 San Sebastian, Basqua Country, Spain

³ Institut für Festkörpertheorie und Theoretische Optik, Friedrich-Schiller-Universität Jena, Max-Wien-Platz 1, 07743 Jena, Germany

E-mail: maurizia.palumbo@roma2.infn.it

Received 20 April 2004

Published 17 September 2004

Online at stacks.iop.org/JPhysCM/16/S4313

doi:10.1088/0953-8984/16/39/006

Abstract

In this paper we review the first-principles theoretical framework of the Bethe–Salpeter equation which is nowadays the state-of-the-art approach for including self-energy, local fields and excitonic effects in the surface optical response. Two different approaches for calculating the dielectric screening will be described. In both cases a parallel and efficient iterative algorithm to find numerically the solution of the BSE equation has been implemented. In fact, if the surface states are not energetically separated from the bulk states and if one is interested in describing a large energy window, the traditional approach involving a full diagonalization of a very large excitonic Hamiltonian is prohibitive. The reflectance anisotropy spectrum of the monohydride Si(100) is considered and compared with experiments. A comparison of the results obtained within different treatments of the electron–hole screening is made. Convergence and numerical problems are discussed.

1. Introduction

In recent years, optical spectroscopies have been more and more involved in experimental *in situ* surface studies because they are non-damaging, they allow the study of surfaces even under non-ultrahigh vacuum conditions and are sufficiently fast to follow real time surface modifications. In particular, the technique of reflectance anisotropy spectroscopy (RAS), which measures the anisotropy with respect to light polarization, has shown excellent surface sensitivity. In the case where RAS is used on the surfaces of cubic materials, the bulk contribution to reflectance,

as described by Fresnel formulae, does not depend on the direction of light polarization, whereas the surface contribution, due to the lower symmetry of the surface, may depend on it. Hence, the reflectance difference between measurements carried out with two different light polarizations in the surface plane, the reflectance anisotropy (RA) (typically only a few per cent of the total reflectance), is generated at the surface [1]. However the interpretation of these experiments is generally not straightforward. Hence, the full potential of surface optical spectroscopy, as well as of any other spectroscopy, can be exploited only thanks to a strong interaction between experimental and theoretical work. The contribution of theorists to this collaboration can be of two types:

- (i) to use the calculated optical spectra to identify the geometrical model that better reproduces the experimental results,
- (ii) and to give the theoretical interpretation of the structures observed in the experimental spectra.

In this context we recently assisted in a rapid development of efficient first-principles approaches to the calculation of the optical spectra of bulk materials, nanostructures, clusters and surfaces. Two main approaches have been proposed so far: many-body perturbation theory (MBPT) [2], and time-dependent density functional theory (TDDFT) [3]. Both open, in principle, a pathway for theoretically correct calculations of optical spectra. The MBPT combines the GW approach for the single quasi-particle states with the solution of the Bethe–Salpeter equation for the excitonic contributions. Calculations based on MBPT have been successfully carried out since the 1980s and it is now a well established methodology. Unfortunately the large numerical effort requested by the different steps of the calculations makes MBPT extremely demanding for systems with many inequivalent atoms. In this paper we will show that using high-performance supercomputers and efficient and parallel algorithms, it is nowadays possible to apply successfully MBPT to surfaces.

An alternative approach for computing the neutral excitations is TDDFT, that is expected to be more efficient than the MBPT-based approach. TDDFT is really promising but many conceptual and computational problems remains still unsolved preventing its application to complex systems [4].

For this reason we will focus, in this work, only on the MBPT approach.

2. Theoretical framework

Density functional theory (DFT) [5] is a single-particle approach that has achieved great success in calculating the ground state electronic properties of many-electron systems. However, when physical properties involving excited states are required, this mean-field theory often fails to describe correctly the experiments yielding only a qualitative agreement with the experimental spectra.

It is well known that DFT-LDA eigenvalues are not the physical single-particle states entering in the absorption process. Instead, electron addition or removal energies (such as those measured in photoemission) should be obtained from an equation similar to the Kohn–Sham one in which the true electron self-energy operator Σ appears in the place of the DFT-LDA exchange–correlation potential. A good approximation for Σ is given by Hedin’s GW approach [6] where Σ is written as the product of the Green function G and the screened Coulomb interaction W . The true QP energies, however, are still not sufficient to correctly describe an absorption process, in which electron–hole pairs are created [9]. Their interaction can lead to a dramatic shift of peak positions as well as to distortions of the spectral lineshape. As already shown for systems such as bulk and clusters, the agreement between theoretical

and experimental optical spectra is greatly improved when excitonic effects are included in the calculations [10, 12, 13, 11].

In the following we will resume in more detail the main equations of the three-step procedure used to obtain the macroscopic dielectric tensor of surfaces needed to calculate the reflectance anisotropy spectra [1, 14]. First of all, through a DFT-LDA calculation [5, 15] with the use of norm-conserving pseudopotentials [16, 17], the geometrical structure of the relaxed ground state configuration of the surface is obtained by solving self-consistently the Kohn–Sham equations:

$$[-\frac{1}{2}\nabla^2 + V_{\text{eff}}^{\text{KS}}(\mathbf{r})]\phi_i(\mathbf{r}) = \epsilon_i\phi_i(\mathbf{r}) \quad (1)$$

where $V_{\text{eff}}^{\text{KS}}(\mathbf{r}) = V_{\text{ext}}(\mathbf{r}) + V_{\text{H}}(\mathbf{r}) + V_{\text{xc}}(\mathbf{r})$, with V_{ext} the external potential, V_{H} the Hartree potential and V_{xc} the exchange–correlation of an homogeneous electron gas calculated at the local density $\rho(r) = \sum_i^N |\phi_i(\mathbf{r})|^2$ [15].

The eigenvectors and eigenvalues of the Kohn–Sham equation are then considered as a first approximation to the true electronic wavefunctions and can be used to obtain the dielectric function according to the independent particle picture or IP-RPA (independent particle–random phase approximation) level as a sum over independent contributions from valence–conduction band pairs at different k -points of the Brillouin zone (BZ) [18].

In the second step the one-particle excitation energies are obtained. The DFT-LDA eigenvalues are corrected by solving the quasiparticle equation within the GW approximation. This equation is formally similar to the Kohn–Sham equation but in place of the local, energy independent exchange–correlation DFT potential the self-energy operator (which is non-Hermitian, non-local and energy dependent) appears [19]:

$$(-\frac{1}{2}\nabla^2 + V^{\text{ext}} + V^{\text{H}})\Psi_i(\vec{r}, \omega) + \int \Sigma(\vec{r}, \vec{r}', \omega)\Psi_i(\vec{r}', \omega) d\vec{r}' = E_i(\omega)\Psi_i(\vec{r}). \quad (2)$$

The calculated quasi-particle energies (i.e. the excitation energies) are the output of this part of the calculation and with the full dielectric matrix calculated within the random phase approximation (RPA) at the DFT level they are used as an input for the third step, which is the solution of the two-particle Bethe–Salpeter equation. Using the GW corrected energies instead of DFT-LDA eigenvalues the dielectric matrix can be calculated in an independent quasiparticle picture (IQ-GW-RPA) [20].

Equation (2) is not usually solved directly thanks to the fact that the Kohn–Sham wavefunctions are often very similar to the GW ones making it sufficient to calculate the QP correction in first-order perturbation theory [7, 8]. The energy dependence of the self-energy is accounted for expanding Σ in Taylor series. The QP corrections are then given by

$$\Delta\epsilon_{nk} = \frac{1}{1 + \beta_{nk}} \langle \phi_{nk}^{\text{LDA}} | \Sigma(\epsilon_{nk}^{\text{LDA}}) - V_{\text{xc}}^{\text{LDA}} | \phi_{nk}^{\text{LDA}} \rangle \quad (3)$$

where β_{nk} is the linear coefficient in the energy expansion of Σ around the DFT-LDA eigenvalues ϵ_{nk} .

The third step is the solution of the Bethe–Salpeter equation (BSE), that describes the electron–hole pair dynamics. As well explained in the literature [4], the BSE can be written as a linear problem whose Hamiltonian is given by

$$H_{\text{exc}}^{(n_1, n_2), (n_3, n_4)} = (E_{n_2}^{\text{QP}} - E_{n_1}^{\text{QP}})\delta_{n_1, n_3}\delta_{n_2, n_4} - i(f_{n_2} - f_{n_1}) \times \int d\mathbf{r}_1 d\mathbf{r}'_1 d\mathbf{r}_2 d\mathbf{r}'_2 \\ \times \phi_{n_1}(\mathbf{r}_1)\phi_{n_2}^*(\mathbf{r}'_1)\Xi(\mathbf{r}_1, \mathbf{r}'_1, \mathbf{r}_2, \mathbf{r}'_2)\phi_{n_3}^*(\mathbf{r}_2)\phi_{n_4}(\mathbf{r}'_2) \quad (4)$$

where f_{n_i} are the occupation numbers (denoting band index and wavevector), $E_{n_2}^{\text{QP}}$ and $E_{n_1}^{\text{QP}}$ are the quasi-particle eigenvalues and ϕ_{n_i} are the Kohn–Sham one-particle wavefunctions. The

kernel Ξ contains two contributions: \bar{v} , which is the bare Coulomb interaction where the long range part corresponding to vanishing wavevector is eliminated, and W , the attractive screened Coulomb electron–hole interaction. The first term describes local field effects and is exactly equivalent to the Adler–Wiser approach when the electron–hole attraction W is neglected [4, 23]. This excitonic Hamiltonian is not Hermitian but, as shown in the literature [12], it is possible to consider only its resonant part (n_2 labelling an empty state, n_1 labelling a filled state), recovering the Hermiticity and reducing the dimension by a factor of two.

The resonant part of H_{exc} , written in the reciprocal space, is

$$H_{\text{exc}}^{\text{res}(vc\mathbf{k}), (v'c'\mathbf{k})} = (E_{c\mathbf{k}}^{\text{QP}} - E_{v\mathbf{k}}^{\text{QP}}) \delta_{vv'} \delta_{cc'} \delta_{\mathbf{k}, \mathbf{k}'} + \frac{4\pi}{\Omega} \sum_{\mathbf{G}, \mathbf{G}'} \left\{ 2 \frac{\delta_{\mathbf{G}, \mathbf{G}'} (1 - \delta_{\mathbf{G}, 0})}{|\mathbf{G}|^2} B_{cv}^{\mathbf{k}\mathbf{k}'}(\mathbf{G}) B_{c'v'}^{\mathbf{k}', \mathbf{k}'*}(\mathbf{G}) \right. \\ \left. - \frac{\epsilon^{-1}(\mathbf{k} - \mathbf{k}' + \mathbf{G}, \mathbf{k} - \mathbf{k}' + \mathbf{G}', \omega = 0)}{|\mathbf{k} - \mathbf{k}' - \mathbf{G}|^2} B_{cc'}^{\mathbf{k}\mathbf{k}'}(\mathbf{G}) B_{vv'}^{\mathbf{k}, \mathbf{k}'*}(\mathbf{G}') \right\} \quad (5)$$

where

$$B_{n,n'}^{\mathbf{k}, \mathbf{k}'}(\mathbf{G}) = \frac{1}{\Omega} \int d^3r u_{n\mathbf{k}}(r) u_{n'\mathbf{k}'}(r) e^{i\mathbf{G}r}$$

is the Bloch integral, u is the periodic part of the Bloch wavefunctions and Ω is the volume of the unit cell.

3. Numerical details

In this paragraph we discuss the numerical details and evidenciate the existing differences between the two numerical approaches used in this work. A detailed discussion of the theoretical results, and their comparison with experiments for the monohydride Si(100), will be given in the following paragraph. The results, illustrated in figures 1–3, are obtained by modelling the monohydride Si(100) surface with a repeated slab containing 12 atomic layers and an equivalent vacuum region, while figures 4 and 5 show the results obtained within the first computational approach but with a repeated slab of 16 atomic layers. Norm-conserving pseudopotentials [16, 17] for Si and H atoms have been employed in both cases. Four \bar{k} -points in the irreducible part of the surface Brillouin zone are used for the self-consistent calculation of the ground-state charge density. In order to make the excitonic calculation feasible, 200 uniformly distributed k -points have been used, although they are not sufficient to give a complete convergence with respect to the correct sampling of the two-particle density of states.

The three numerical steps are implemented in different ways. In order to distinguish the two calculations, we will refer to method A for the first, and to method B for the second one. In method A, the DFT-LDA electronic structure has been calculated within a plane-wave code [29], while in the second, B, a real space finite-difference code [28] has been used.

We checked that by employing the same slab thickness and number of \bar{k} -points, the repeated slab dielectric functions at the IQ-RPA level, obtained within the two different approaches, were equal.

Regarding the GW part, the major bottleneck is the computation of the screened interaction W . In order to reduce the computational effort we followed different strategies in the two calculations. In the first case (method A), thanks to our past experience of full GW calculations for the Si(100) surface [21] and to the H saturation of the surface Si dangling bonds, we hypothesized a small dispersion of the self-energy corrections, and we approximated them with a rigid scissor operator of 0.6 eV. In the second case (method B), a substantial improvement in speed has been achieved by using a model dielectric function. A functional form proposed by Bechstedt *et al* [22], which reproduces very well the random-phase approximation for bulk

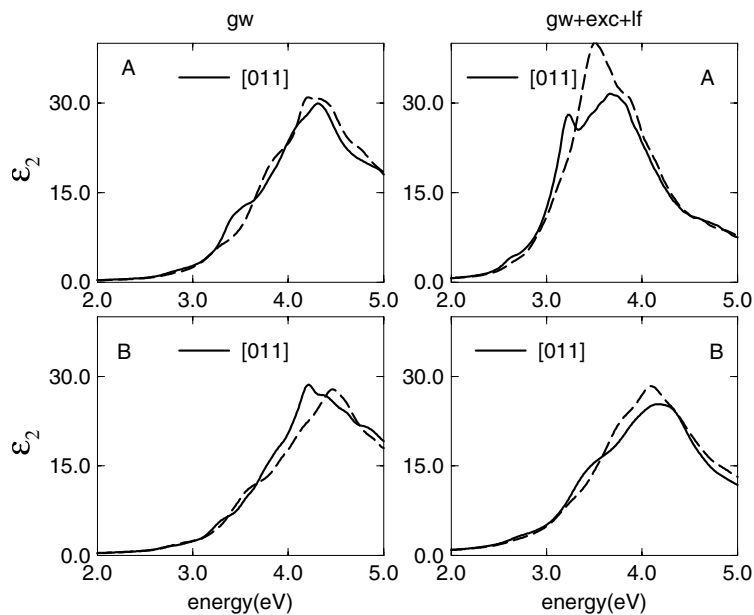


Figure 1. Surface dielectric functions of monohydride Si(100) 2×1 surface for light polarized along the dimers (full curves) and in the perpendicular direction (dashed curves). Left panels: IQ-GW-RPA curves: method A (upper panel); method B (lower panel). Right panels: curves obtained including self-energy, local fields and excitonic effects within method A (upper panel) and method B (lower panel).

semiconductors, has been used. Moreover, local field effects are approximately described using homogeneous state-averaged densities as in [22].

The electron–hole screening term, in the excitonic matrix, is also treated in different ways in the two methods: in method A the inverse of the full RPA static dielectric matrix is used, while in method B the same model dielectric function as used in the GW step is applied.

Moreover, in order to eliminate the need to diagonalize [12] the very large non-sparse excitonic matrix (of order of $100\,000 \times 100\,000$), two different numerical methods have been implemented: in method A we implemented, in a parallel version, the Haydock iterative algorithm proposed by Shirley a few years ago in order to solve the Bethe–Salpeter equation [24]. The construction of the excitonic Hamiltonian and the matrix–vector products needed to apply the Haydock approach are distributed among different processors. In method B, the macroscopic polarizability is obtained from the solution of an initial-value problem [25, 27].

4. Results and discussion

In figure 1 we compare the 12-atomic-layer repeated slab dielectric functions, obtained within method A and method B, for light polarized along the two perpendicular directions in the surface plane. In the left panels, we show the IQ-GW-RPA curves obtained within the two methods (A, upper panel; B, lower panel). The same comparison, but including self-energy, local-field and excitonic effects, is made in the right panels.

The first point we want to stress is the different behaviour of the GW calculations. In method A, due to the rigid shift applied to the conduction bands, the GW curves are only blue-shifted with respect to the DFT-LDA ones, while in the second numerical approach (method B)

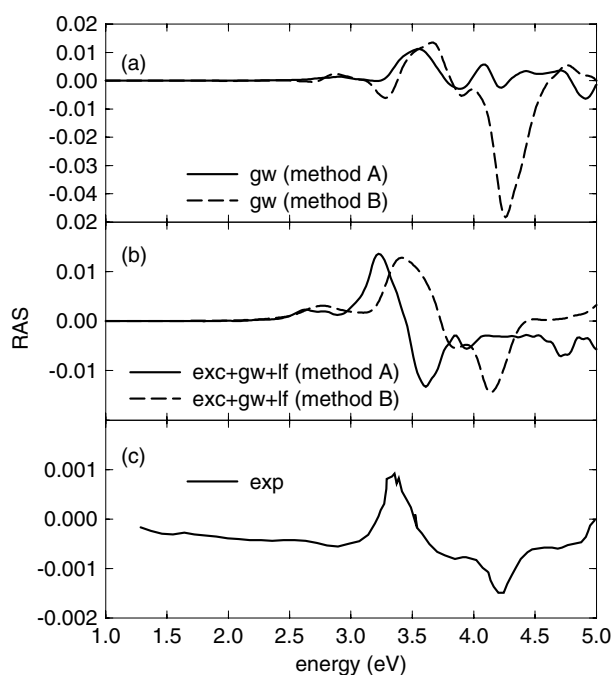


Figure 2. Reflectance anisotropy spectra of the monohydride Si(100) surface. Upper panel: IQ-GW-RPA spectra; solid curve, method A; dashed curve, method B. Central panel: spectra with self-energy, local field and excitonic effects included (GW + LF + Exc); solid curve, method A; dashed curve, method B. Lower panel: experimental spectrum from [26].

the simplified GW method also produces a change in shape of the curves, probably due to an overestimation of the self-energy correction dispersion. On the other hand, the rigid shift seems to underestimate the peak positions related to the bulk-like critical points E_1 , E'_0 and E_2 by about 0.3–0.5 eV.

The different approach to calculating W also influences the excitonic part of the calculations, as evident in the right panels of the same figure: in method A, important anisotropic excitonic effects appear (upper right panel); in method B, these effects are smaller, leading essentially to a red-shift of the curves, without really affecting much their shape (lower right panel).

In figure 2 the experimental RA spectrum (panel (c)) [26] is compared with the theoretical results. The measured signal is characterized by positive and negative peaks around 3.4 and 4.3 eV. At these energies, the critical points of the bulk electronic responses, the E_1 and E_2 structures occur. Therefore, the optical anisotropy of the hydrogen-terminated Si(100) surface is explained as modulation of the bulk dielectric function. Moreover, since the dimer-related surface states have been removed from the fundamental gap region and the characteristic spectral features appear at the energies of the bulk critical points, a large number of surface-modified bulk states also contribute to the surface optical response. Consequently, from a theoretical point of view, a large number of electron–hole pairs need to be included in the calculation. Before starting to comment on the theoretical RAS we want to stress that the presence of more structures with respect to the experiment is due to the numerical noise produced by the limited thickness of the slab and by the finite k -point mesh and, for calculations with excitonic effects included, also by the limited number of electron–hole transitions considered (this effect is particularly evident in the solid curve of figure 5).

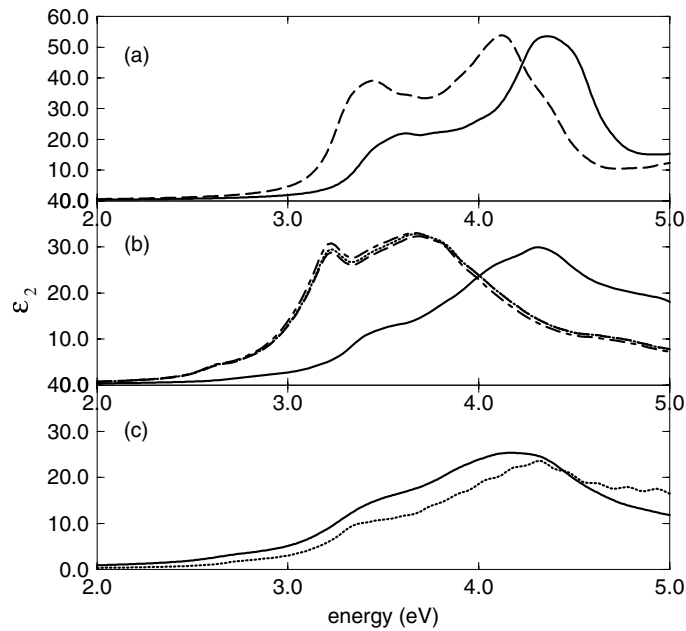


Figure 3. Upper panel, $\epsilon_2(\omega)$ for bulk Si, obtained including self-energy correction (solid curve) and GW, LF and excitonic effects (dashed curve); central panel, (110) component of the imaginary part of the dielectric response of the repeated slab; GW level (solid curve) GW + LF + Exc, $1100 \times 1100G$ and 50 occupied and 50 unoccupied bands mixed in the excitonic matrix (dashed curve), GW + LF + Exc with different numbers involved, only 30 occupied and 40 unoccupied (dotted curve), and a different dimension of the screening matrix ($700G \times 700G$) (dot-dashed curve). Lower panel: the same component of the dielectric tensor of central panel is reported but obtained within method B (solid curve) and within method A but with a simple form of the screening (see the text).

The IP-RPA spectra obtained within the two numerical approaches (methods A and B) described in the text are not reported in this paper because they coincide with the DFT-LDA spectrum of [27].

In figure 2(a) we plot the IQ-GW-RPA spectra obtained within the two methods. Important differences above 4 eV do appear: while with method B an intense negative peak appears [27], within method A this peak is almost completely absent.

In figure 2(b) the complete theoretical RAS curves obtained with method A (solid curve) and method B (dashed curve) are reported. In both cases an improvement with respect to the GW curves is obtained below 4 eV. In the second case the negative peak at about 4.3 eV, which grows up in the GW part of the calculation, is still present and a good agreement with the experiment is reached. In the first approach however, a big negative peak is present at 3.7 eV while the lack of a negative peak (at the GW level) at about 4.3 eV remains even when excitonic effects are included. Comparing these results with the experimental curve [26], shown in the lower panel, we can deduce the following: at the GW level, approach A probably underestimates the quasi-particle band dispersion while approach B overestimates it. In the screening calculation of the excitonic matrix, the opposite behaviour seems to occur.

Furthermore, we plot figure 3 with a double purpose: on one hand we want to compare the bulk with the repeated slab $\epsilon_2(\omega)$ obtained within methods A and B; on the other hand we want to show that the convergence with the number of the electron–hole transitions and the

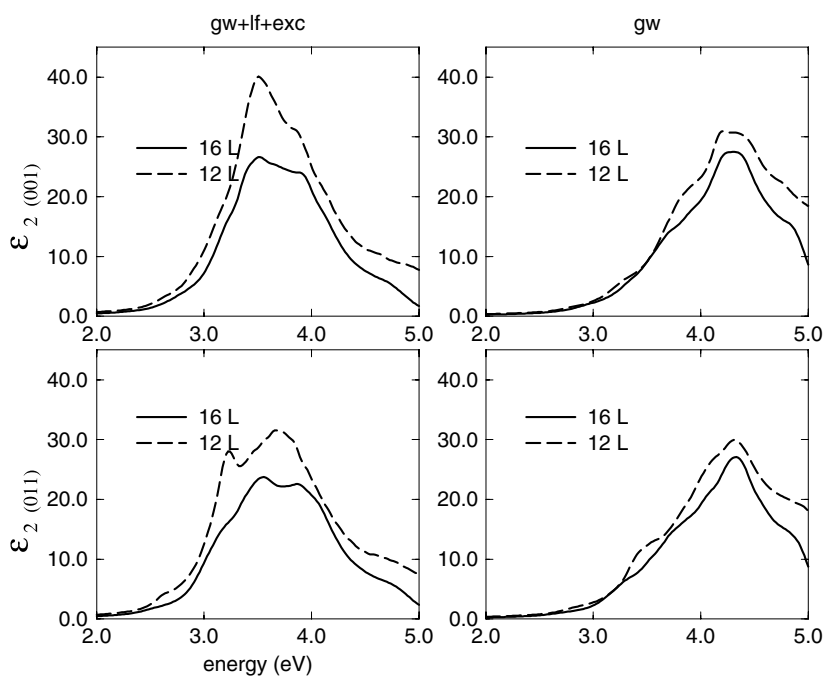


Figure 4. Theoretical imaginary part of the surface dielectric functions for light polarized along the dimers (lower panels) and in the perpendicular direction (upper panels) obtained within method A. IQ-GW-RPA results: solid curve, 16 atomic layers; dashed curve, 12 atomic layers. Curves obtained including self-energy, local fields and excitonic effects: solid curve, 16 atomic layers; dashed curve, 12 atomic layers.

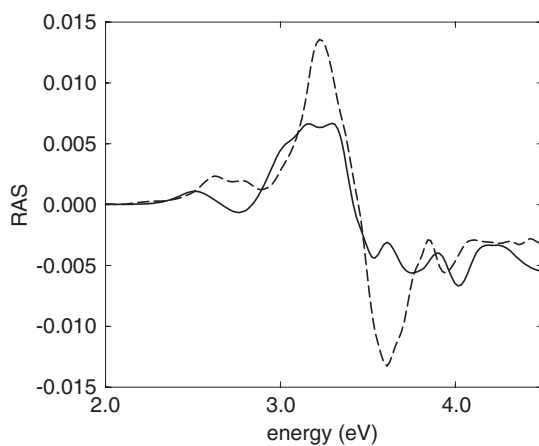


Figure 5. Theoretical RAS obtained, within method A, including self-energy, local-field and excitonic effects for slabs of 12 atomic layers (dashed curve) and 16 atomic layers (solid curve).

dimension (in G-space) of the screening matrix, in the electron-hole Coulomb attractive term, has been tested.

In figure 3(a) we show the imaginary part of the bulk dielectric function obtained at the GW-RPA level (solid curve) and including GW, LF and excitonic effects (dashed curve) in order to compare them with the corresponding curves of the Si(100):2H repeated slab (for light

polarization along the dimers; central panel). In the central panel, different curves (obtained with method A, but with different sets of transitions and plane wave expansions in the excitonic matrix) are reported to show the convergence behaviour and also to compare them with the corresponding bulk curves (upper panel). In the lower panel (figure 3(c)) we plot $\epsilon_2(\omega)$, obtained within the first numerical approach (method A), but replacing the full RPA W with the simple form of $W = 1/\epsilon_{\text{inf}}^{\text{bulk}} r$ with $\epsilon_{\text{inf}}^{\text{bulk}} = 11.4$ and we compare it with the curve obtained within the second numerical approach B.

This result suggests that the way in which the screening is calculated is crucial in the final contribution to the excitonic effects at a surface, which are strongly reduced when a non-full-RPA dielectric function is used.

Finally, in order to understand if the important excitonic effects, observed in method A, are influenced by the thickness of the slab, we repeated the computational procedure for a 16-atomic-layer slab (with the same vacuum region). Figure 4 shows the comparison of 12 and 16 atomic layers $\epsilon_2(\omega)$, at the GW (right panels) and GW + LF + Exc level (left panels). Although moving from a 12- to 16-layer thickness results in a reduction of the excitonic effects, the peak energy positions remain different from the results obtained within method B.

In figure 5 the theoretical RAS obtained at the end of the three-step procedure is reported. An improvement in the 16-layer calculation is observed: a low energy negative structure, also observed experimentally, appears. We also notice the presence of a new negative structure at about 4.3 eV, and the disappearance of the negative peak at 3.7 eV, not present in the experiment. This curve is qualitatively similar to that of method B, calculated for a 12-layer slab, shown in figure 2(b).

5. Conclusions

The two methods employed here to calculate excitonic effects are based on different approximations. Method A seems to underestimate GW corrections with respect to method B, while it overestimates the excitonic effects. The RAS spectra calculated within the two methods for a 12-layer slab, shown in the central panel of figure 2, show similar lineshapes but are shifted in energy with respect to each other. We believe this to be due to an overestimation of the electron–hole interaction (screened by the slab dielectric function) in thin slabs within method A, which does not occur within method B as a consequence of the larger screening: in fact, in method B, the e–h interaction is basically screened by the bulk dielectric function, which is larger than the slab one; this is demonstrated by the similarity of the two curves in the lowest panel of figure 3 (one with bulk screening, the other with that of method B). However, when the slab thickness increases up to 16 layers, the e–h interaction of method A decreases, leading to a final RAS curve more similar to that of method B and to the experiment. In conclusion, method A (more rigorous) and method B (less rigorous but faster), in the case of Si(100):2H, lead to similar RAS curves when reasonable convergences are achieved within each method. A calculation of the RAS of surfaces involving several pairs of valence and conduction bands (such as Si(100):2H), including excitonic effects, is feasible at present, although computationally very demanding. Our calculations show that surface optical properties can indeed be calculated taking into account quasiparticle, excitonic and local-field effects. However, one has to go to the limits of the computational possibilities. As a consequence, some quantities entering the calculations, e.g. the screening, have to be described either by not fully converged calculations or within certain approximations. For this purpose, to improve this situation, one has to wait for the development of more efficient computers and/or methodologies such as TDDFT [30–32], which should allow us to treat more k -points, thicker slabs and more realistic dielectric functions.

Acknowledgments

This work has been supported by the PAIS INFM CELEX, MIUR-COFIN 2002, and by the EU through the Nanophase Research Training Network (contract No HPRN-CT-2000-00167). We acknowledge CINECA CPU time granted by INFM. We thank Lucia Reining and Valerio Olevano for useful discussions and Conor Hogan for a careful reading of the manuscript.

References

- [1] Del Sole R 1995 *Photonic Probes of Surfaces* ed P Halevi (Amsterdam: Elsevier) p 131 and references therein
- [2] Fetter A L and Walecka J D 1971 *Quantum Theory of Many-Particle Systems* (New York: McGraw-Hill)
- [3] Runge E and Gross E K U 1984 *Phys. Rev. Lett.* **52** 997
- [4] Onida G, Reining L and Rubio A 2002 *Rev. Mod. Phys.* **5** 74 601
- [5] Hohenberg P and Kohn W 1964 *Phys. Rev.* **136** B864
Kohn W and Sham L J 1965 *Phys. Rev.* **140** A1113
- [6] Hedin L 1965 *Phys. Rev.* **139** A796
- [7] Hybertsen M S and Louie S G 1986 *Phys. Rev. B* **34** 5390
- [8] Godby R W, Schlüter M and Sham L J 1988 *Phys. Rev. B* **37** 10159
- [9] Hanke W 1978 *Adv. Phys.* **27** 287
- [10] Onida G, Reining L, Godby R W, Del Sole R and Andreoni W 1995 *Phys. Rev. Lett.* **75** 818
- [11] Rohlfing M and Louie S G 1998 *Phys. Rev. Lett.* **80** 3320
- [12] Albrecht S, Reining L, Del Sole R and Onida G 1998 *Phys. Rev. Lett.* **80** 4510
- [13] Benedict L X, Shirley E L and Bohn R B 1998 *Phys. Rev. Lett.* **80** 4514
- [14] Del Sole R and Fiorino E 1984 *Phys. Rev. B* **29** 4631
- [15] Ceperley D M and Alder B J 1980 *Phys. Rev. Lett.* **45** 566
Perdew J P and Zunger A 1981 *Phys. Rev. B* **23** 5048
- [16] Troullier N and Martins J L 1991 *Phys. Rev. B* **43** 19993
- [17] Hamann D R 1989 *Phys. Rev. B* **40** 2980
- [18] Bassani F and Pastori Parravicini G 1975 *Electronic States and Optical Transitions in Solids*
ed R A Ballinger (Oxford: Pergamon) p 177
- [19] Aryasetiawan F and Gunnarsson O 1998 *Rep. Prog. Phys.* **61** 237
Johsson A W G and Wilkins J W 1999 *Solid State Physics* ed H Ehrenreich and F Spaepen (New York: Academic)
- [20] Del Sole R and Giralda R 1996 *Phys. Rev. B* **54** 14376
Del Sole R and Giralda R 1993 *Phys. Rev. B* **48** 11789
- [21] Pulci O, Power J, Shkrebtii A I, Richter W and Del Sole R 2004 *Comput. Mater. Sci.* **30** 98
Power J, Pulci O, Shkrebtii A I, Galata S, Astropekkakis A, Hinrichs K, Esser N, Del Sole R and Richter W 2003
Phys. Rev. B **67** 115315
- [22] Bechstedt F, Del Sole R, Cappellini G and Reining L 1992 *Solid State Commun.* **84** 765
- [23] Adler S L 1962 *Phys. Rev.* **126** 413
Wiser N 1963 *Phys. Rev.* **129** 62
- [24] Benedict L X and Shirley E L 1999 *Phys. Rev. B* **59** 5441
- [25] Hahn P H, Schmidt W G and Bechstedt F 2002 *Phys. Rev. Lett.* **88** 016402
- [26] Shioda R and van der Weide J 1998 *Appl. Surf. Sci.* **130–132** 266
- [27] Schmidt W G, Glutsch S, Hahn P H and Bechstedt F 2003 *Phys. Rev. B* **67** 085307
- [28] Briggs E L, Sullivan D J and Bernholc J 1996 *Phys. Rev. B* **54** 14362
available under <http://nemo.physics.ncsu.edu/software/MGDFT-QMD/index.html>
- [29] Gonze X, Beuken J-M, Caracas R, Detraux F, Fuchs M, Rignanese G-M, Sindic L, Verstraete M, Zerah G, Jollet F,
Torrent M, Roy A, Mikami M, Ghosez Ph, Raty J-Y and Allan D C 2002 First-principles computation of
material properties: the ABINIT software project *Comput. Mater. Sci.* **25** 478
code available under <http://www.abinit.org>
- [30] Sottile F, Olevano V and Reining L 2003 *Phys. Rev. Lett.* **91** 056402
- [31] Adragna G, Del Sole R and Marini A 2003 *Phys. Rev. B* **68** 165108
- [32] Marini A, Del Sole R and Rubio A 2003 *Phys. Rev. Lett.* **91** 256402